Hindawi Publishing Corporation
Journal of Nanomaterials
Volume 2015, Article ID 514173, 8 pages
http://dx.doi.org/10.1155/2015/514173

Research Article

Sol-Gel Derived Eu^{3+}-Doped $Gd_2Ti_2O_7$ Pyrochlore Nanopowders

Sanja Ćulubrk, Željka Antić, Vesna Lojpur, Milena Marinović-Cincović, and Miroslav D. Dramićanin

Vinča Institute of Nuclear Sciences, University of Belgrade, P.O. Box 522, 11001 Belgrade, Serbia

Correspondence should be addressed to Željka Antić; zeljkaa@gmail.com

Received 4 December 2014; Revised 10 February 2015; Accepted 11 February 2015

Academic Editor: Alan K. T. Lau

Herein we presented hydrolytic sol-gel synthesis and photoluminescent properties of Eu^{3+}-doped $Gd_2Ti_2O_7$ pyrochlore nanopowders. According to $Gd_2Ti_2O_7$ precursor gel thermal analysis a temperature of 840°C is identified for the formation of the crystalline pyrochlore phase. Obtained samples were systematically characterized by powder X-ray diffraction, scanning and transmission electron microscopy, and photoluminescence spectroscopy. The powders consist of well-crystalline cubic nanocrystallites of approximately 20 nm in size as evidenced from X-ray diffraction. The scanning and transmission electron microscopy shows that investigated Eu^{3+}-doped $Gd_2Ti_2O_7$ nanopowders consist of compact, dense aggregates composed entirely of nanoparticles with variable both shape and dimension. The influence of Eu^{3+} ions concentration on the optical properties, namely, photoluminescence emission and decay time, is measured and discussed. Emission intensity as a function of Eu^{3+} ions concentration shows that $Gd_2Ti_2O_7$ host can accept Eu^{3+} ions in concentrations up to 10 at.%. On the other hand, lifetime values are similar up to 3 at.% (~2.7 ms) and experience decrease at higher concentrations (2.4 ms for 10 at.% Eu^{3+}). Moreover, photoluminescent spectra and lifetime values clearly revealed presence of structural defects in sol-gel derived materials proposing photoluminescent spectroscopy as a sensitive tool for monitoring structural changes in both steady state and lifetime domains.

1. Introduction

The insulating rare-earth titanate pyrochlore oxides described by the general formula $RE_2Ti_2O_7$ (RE = Ln^{3+}, Sc^{3+}, or Y^{3+}) have the face-centered cubic crystal structure with the space group $Fd\bar{3}m$. In the structure RE^{3+} and Ti^{4+} ions occupy 16d and 16c sites, respectively, with the D_{3d} symmetry. Due to the ability to accept rare-earth elements in high concentrations, chemical stability, and the fact that they do not show electronic conductivity at ordinary temperatures, rare-earth titanate pyrochlores could be proposed as a potential phosphor and laser host materials. However, due to their unusual structural, magnetic, and electrical conductivity properties most of the research in this field is done on the structural trends [1], thermodynamic and dynamic magnetic properties [2–4], disorders [5, 6], and nonstoichiometry [7].

Many synthesis approaches for rare-earth pyrochlores such as solid state [8–10], sol-gel [11, 12], molten salt [13], hydrothermal [14], stearic acid method [15], and Pechini process [16] have been developed. Among them sol-gel method has been considered as a low cost approach for the preparation of novel nanostructured materials. It is a wet-chemical technique widely used in the fields of materials science and engineering for the fabrication of materials starting from a chemical solution—sol which acts as the precursor for an integrated network of discrete particles—gel. It refers broadly to the room temperature solution routes and enables synthesis of materials with desirable hardness, optical transparency, chemical durability, tailored porosity, and thermal resistance.

In this paper, Eu^{3+}-doped $Gd_2Ti_2O_7$ nanopowders with different dopant concentrations (0.5; 1; 3; 5; 7; 10; and 15 at.% with respect to Gd) were fabricated using sol-gel technique. There are two reasons for using europium. Firstly, it provides an intense red emission and therefore $Gd_2Ti_2O_7$ powders are new red nanophosphors. Secondly, due to nondegenerated ground ($^7F_0$) and excited ($^5D_0$) states together with nonoverlapping $^{2S+1}L_J$ multiplets that give emission spectra with clear dependence on the host material structure and site symmetry, Eu^{3+} is well-known structural probe ion [17, 18]. In this way photoluminescent spectroscopy could be used

as a structural probe technique. The thermal decomposition behavior and proper sintering temperature of the $Gd_2Ti_2O_7$ samples are determined using thermogravimetric/differential thermal analysis (TG-DTA). Fourier transform infrared spectroscopy (FTIR) is used to identify the changes taking place within the precursor gel during drying and calcination. Detailed structural and morphological characterization of the nanocrystalline powders was performed using X-ray diffraction (XRD), scanning (SEM), and transmission electron microscopy (TEM). Optical properties were determined by photoluminescence (PL) excitation, emission, and lifetime measurements. The doping concentrations were systematically investigated in order to obtain the pure phase pyrochlore structure, strongest photoluminescent intensity, and the longest lifetime.

So far there is a lack in reports on photoluminescent properties of rare-earth doped $Gd_2Ti_2O_7$ powders. To date, photoluminescent properties of Eu^{3+}-doped $Gd_2Ti_2O_7$ have been investigated by others in thin film [19], core-shell [20], and nanocomposite [21] form or codoped with V^{4+} ions in powder form [11, 22, 23]. Our previous article reported photoluminescent properties of Sm^{3+} and Eu^{3+}-doped $Gd_2Ti_2O_7$ [16] obtained by mixed metal-citric acid synthesis and this study is the continuation of our research on the rare-earth doped $Gd_2Ti_2O_7$ powders. Moreover, aim of this report is to introduce luminescent spectroscopy as a sensitive tool for monitoring structural changes.

2. Materials and Methods

2.1. Synthesis of $Gd_2Ti_2O_7$:Eu^{3+} Nanoparticles. To produce undoped and Eu^{3+}-doped pyrochlore $Gd_2Ti_2O_7$ in the form of nanopowders the hydrolytic sol-gel route has been adopted, starting from rare-earth nitrates and titanium(IV)-isopropoxide. For the synthesis titanium(IV)-isopropoxide (Alfa Aesar, 97%), water, ethanol, and nitric acid were mixed in molar ratio of 1 : 3 : 20 : 0.08 [24]. In the first step, stoichiometric quantities of $Gd(NO_3)_3 * 6H_2O$ (Alfa Aesar, 99.9%) and Eu_2O_3 (Alfa Aesar, 99.9%) were dissolved in appropriate amount of water and HNO_3. Then titanium(IV)-isopropoxide was dissolved in ethanol under constant magnetic stirring and added to the rare-earth nitrates mixture. For undoped sample only appropriate amount of $Gd(NO_3)_3$ was used. Transparent gels were obtained within few minutes and dried at 70°C for 5 h under atmospheric pressure. In order to obtain pure phase $Gd_2Ti_2O_7$ nanoparticles the undoped and Eu^{+3}-doped dried gels were calcinated at 840°C for 4 hours followed by natural furnace cooling to room temperature. The calcination temperature is chosen according to TG/DTA analysis, the results of which are presented in Section 3.1. Finally, undoped $Gd_2Ti_2O_7$ and 7 $Gd_2Ti_2O_7$ samples doped with x at.% Eu^{3+} (x = 0.5; 1; 3; 5; 7; 10; and 15 with respect to Gd^{3+}) were synthesized.

2.2. Instruments and Measurements. TG/DTA analysis was performed on the SETARAM SETSYS Evolution-1750 instrument. The $Gd_2Ti_2O_7$ dried gel (~10–15 mg) was heated at 10°C min^{-1} heating rate, in air atmosphere (air flow 16 mL min^{-1}), from 30 to 1000°C. Fourier transmission infrared (FTIR) measurements were carried out on the Thermo Nicolet 380 FT-IR instrument, in a reflection mode with a resolution of 4 cm^{-1}. X-ray diffraction (XRD) measurements were performed using Rigaku SmartLab diffractometer. Diffraction data were recorded in a 2θ range from 10° to 90°, counting 0.7°/minute in 0.02° steps. Relevant results of structural analysis (unit cell parameter, crystal coherence size, microstrain values, and data fit parameters) were obtained using built-in package software. Microstructural characterization was done using a JEOL JSM–6610LV scanning electron microscope (SEM) with an acceleration voltage of 20 kV. Microstructure at a local level was analyzed by transmission electron microscopy (TEM) using JEOL-JEM 2100 LaB_6 operated at 200 kV.

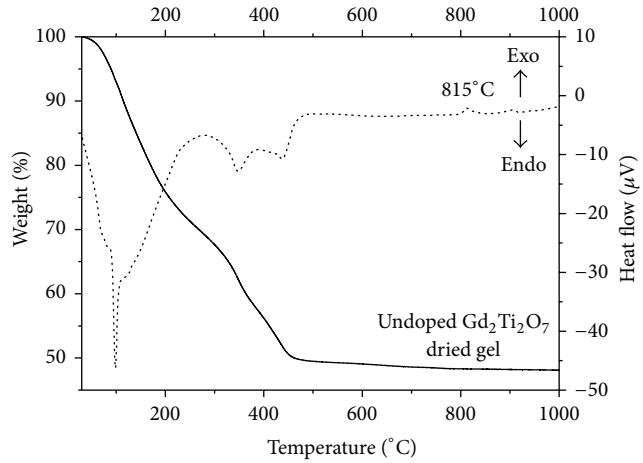

Figure 1: Thermogravimetry (TG, solid line) and differential thermal analysis (DTA, dotted line) curves for undoped $Gd_2Ti_2O_7$ dried gel (70°C for 5 h).

Photoluminescence (PL) measurements were performed under room temperature conditions. Measurements were done on Fluorolog-3 Model FL3-221 spectrofluorometer system (Horiba Jobin-Yvon), utilizing 450W Xenon lamp as excitation source for emission measurements and Xenon-Mercury pulsed lamp for lifetime measurements. TBX-04-D PMT detector is used for both lifetime and steady state acquisitions. The line intensities and positions of the measured spectra were calibrated with a standard mercury-argon lamp. All photoluminescence measurements were performed on pellets prepared from the powders under a load of 5 tons and without any additives.

3. Results and Discussion

3.1. Thermal Analysis (TG/DTA). The $Gd_2Ti_2O_7$ gels prepared with hydrolytic sol-gel route were of amorphous nature and under appropriate sintering they transformed to crystalline $Gd_2Ti_2O_7$. Thermal analysis of dried gel was performed in order to determine proper sintering temperature for the transformation to pyrochlore phase. Results of TG/DTA analysis clarified the existence of three temperature regions (see Figure 1). Between room temperature and 275°C

Table 1: Characteristic vibrational modes obtained from FTIR measurements.

Functional group	Region (cm^{-1})	Comments
-OH stretching vibration	3600–3000	From water
Aliphatic C-H stretching vibration	3000–2800	From isopropoxide
O-N=O asymmetrical stretching	~1650	From nitrates
Asymmetrical and symmetrical CH_3 deformation vibrations	1450–1350	From isopropoxide
$CH(CH_3)_2$ skeletal vibrations	1170–880	From isopropoxide
N-O stretching vibrations	~800	From nitrates
CO_2	2400–2300	Inevitable in the atmosphere

strong endothermic peak attributed to the vaporization of adsorbed organic molecules occurs in the DTA curve. In the same temperature range the TG curve shows a marked weight loss (~30%). In the second temperature range between 275°C and 500°C two endothermic peaks are indicated by DTA. At the same time weight loss (~20%) indicated by TG could be related to the elimination of the residual organic compounds. In the third region a DTA exothermic peak at ~815°C could be attributed to the amorphous to crystalline transformation of $Gd_2Ti_2O_7$, while after 500°C the mass remains constant. According to these results calcination temperature of 840°C was chosen. Comparing with our previous results on rare-earth doped $Gd_2Ti_2O_7$ obtained with mixed metal-citric acid synthesis (appropriate sintering temperature was ~880°C, [16]) this temperature is somewhat lower. Additionally, more structured shape of TG/DTA curves shows that thermal behavior of sol-gel derived materials is more complex compared to mixed metal-citric acid ones.

According to our previous study on the crystallization of phosphor materials prepared by sol-gel method [25], one should expect that materials crystallize in a two-step process. In the primary crystallization stage nonconstant radial growth rate is present, while in the second stage two-dimensional crystal growth occurs.

3.2. Fourier Transform Infrared Spectroscopy (FTIR). Figure 2 presents the FTIR spectra of undoped $Gd_2Ti_2O_7$ gel, dried gel, and powder obtained after calcination at 840°C for 4 hours. Broad band with a maximum at ~3310 cm^{-1} arises from the stretching vibrations of OH^- groups [26] and is especially visible in the $Gd_2Ti_2O_7$ gel. Many peaks in the gel's and precursor's spectra could be attributed to the organic and nitrate presence (see Table 1, [26]). One can notice that after heat treatment peaks from H_2O, NO_3^- groups and organic disappear completely. Due to formation of new lattice, the main feature of the titanate pyrochlores, the strong band in the range 600–400 cm^{-1} [27], is only visible after thermal treatment at 840°C.

3.3. X-Ray Diffraction (XRD). $Gd_2Ti_2O_7$ pyrochlore crystallizes in the face-centered cubic lattice (space group $Fd\bar{3}m$, number 227) with the unit cell containing eight molecules ($Z = 8$) and four crystallographically nonequivalent sites (Ti at 16c, Gd at 16d, O at 48f, and O′ at 8b). In the studied structure, Ti^{4+} and Gd^{3+} cations (and consequently rare-earth dopants) are situated in a centrosymmetric site of D_{3d} symmetry.

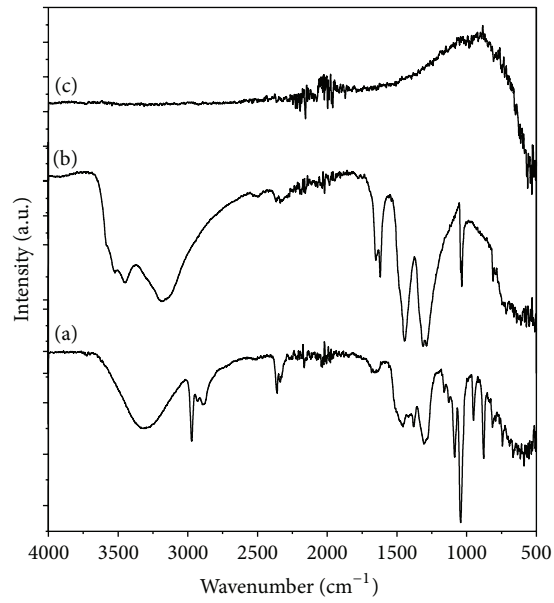

Figure 2: FTIR spectra of undoped $Gd_2Ti_2O_7$: (a) gel, (b) dried gel at 70°C for 5 h, and (c) powder obtained after calcination at 840°C for 4 h.

XRD patterns of undoped and seven Eu^{+3}-doped $Gd_2Ti_2O_7$ powders together with ICDD card number 01-074-9640 are presented in Figures 3(a) and 3(b). No other phase peaks or traces of impurities were detected up to 10 at.% Eu^{3+} indicating that, up to this concentration, dopant Eu^{3+} ions have been effectively incorporated into the $Gd_2Ti_2O_7$ host lattice. However, at 15 at.% Eu^{3+}, barely visible traces of impurities are present. In order to investigate presence of trace impurities in more detail diffractogram of 15 at.% Eu^{3+}-doped sample is recorded under longer acquisition time and presented in Figure 4. Additional diffractions could be assigned to the traces of Ti_5O_9 (ICDD card number 01-075-1815) and Ti_6O_{11} (ICDD card number 01-085-1058). According to the Ti–O phase diagram [28] large number of oxides and suboxides, TiO_2, Ti_6O, Ti_3O, Ti_2O, TiO, Ti_2O_3, and Ti_3O_5, as well as Magnelli phases Ti_nO_{2n-1} ($4 < n < 10$), could be present at 298 K. However, for given stoichiometry, besides TiO_2, most probable is formation of Magnelli phase impurities. Even though amounts of all constituting ions are precisely calculated and weighted, presence of bigger in size dopant Eu^{3+} in high concentration leads to structural misbalance and formation of stoichiometrically close Ti_5O_9 and Ti_6O_{11} impurity phases traces.

Compared to our previous results [16], one can conclude that sol-gel route allows incorporation of Eu^{+3} ions into $Gd_2Ti_2O_7$ host lattice in lower concentrations (up to 10 at.%) compared with mixed metal-citric acid synthesis (up to

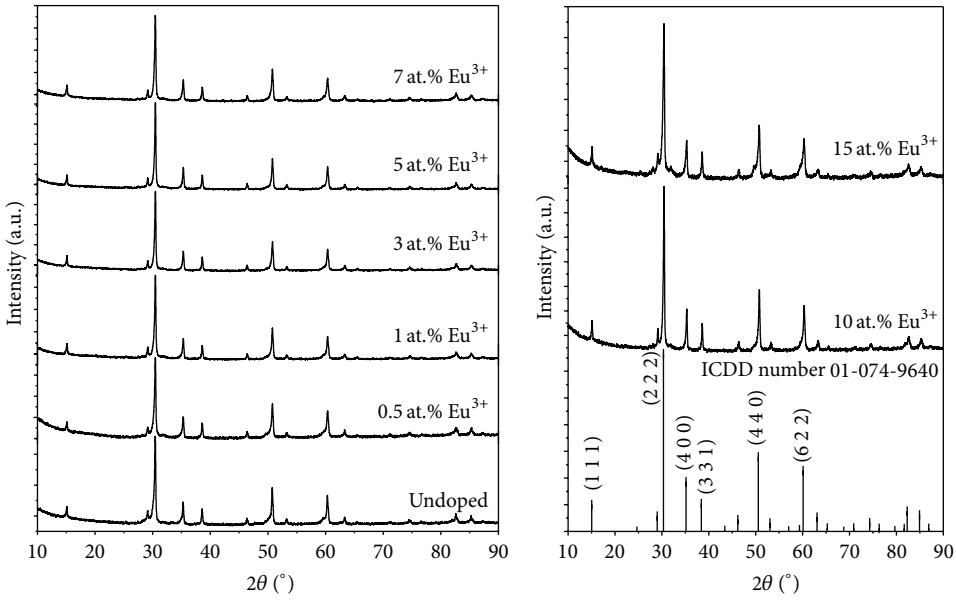

Figure 3: XRD patterns of (a) undoped and Eu^{+3}-doped $Gd_2Ti_2O_7$ powder samples (0.5–7 at.% Eu^{3+}) and (b) 10 at.% and 15 at.% Eu^{3+}-doped $Gd_2Ti_2O_7$ powder samples. The diffraction peaks are indexed according to the presented ICDD card number 01-074-9640.

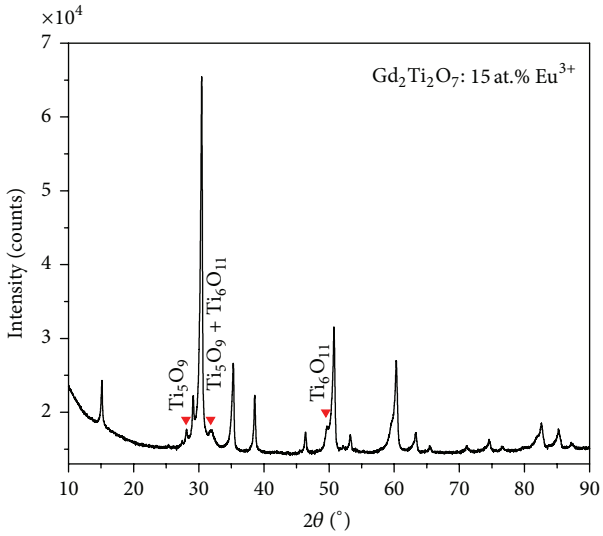

Figure 4: XRD diffractogram of 15 at.% Eu^{3+}-doped sample taken under longer acquisition time. Traces of impurities could be denoted by both Ti_5O_9 (ICDD card number 01-075-1815) and Ti_6O_{11} (ICDD card number 01-085-1058) Magnelli phases.

15 at.%). However, more detailed investigation (between the range of 10 and 15 at.% Eu^{3+}) is necessary to precisely determine the extent to which the Eu^{3+} ion can be accommodated into sol-gel obtained $Gd_2Ti_2O_7$ pyrochlore matrix.

Relevant results of structural analysis (unit cell parameter, crystal coherence size, microstrain values, and data fit parameters) are presented in Table 2. The starting parameters for the structural analysis were taken according to [9]. Unit cell parameter, *a*, increases with rare-earth doping due to replacement of smaller Gd^{3+} (r_{VI}^{3+} = 0.938 Å) with bigger in size Eu^{3+} (r_{VI}^{3+} = 0.947 Å) ion. The largest unit cell parameter was found for the sample with the highest Eu^{3+} dopant concentration (10 at.%). Similar crystallite size of around 20 nm found for all samples shows that dopant concentration does not affect crystallite size. Data fit parameters, the regression sum of relative errors (Rp), the regression sum of weighted squared errors (Rwp), and the goodness of fit (GOF) are small indicating a highly satisfactory reliability. Microstrain values are low suggesting good ion ordering in the nanocrystals.

3.4. Scanning and Transmission Electron Microscopy (SEM/TEM). A SEM study was conducted to investigate the surface morphology of the powders and representative sample images are given in Figures 5(a) and 5(b). The micrographs show that representative 3 at.% Eu^{3+}-doped $Gd_2Ti_2O_7$ consists of compact, dense aggregates composed entirely of nanoparticles. Microstructure at a local level investigated by TEM (Figures 5(c) and 5(d)) revealed that sol-gel synthesis produces powders with irregular both particles size and shape. The nanoparticles are organized in agglomerates, some of which formed the bigger crystals. This was visible for all Eu^{3+}-dopant concentrations as well. The local crystal structure was investigated with the selected area electron diffraction technique (SAED) and one representative ring electron diffraction pattern is presented as Figure 5(c) inset. The presence of rings is the evidence of $Gd_2Ti_2O_7$ polycrystalline nature, while their grainy appearance is connected to the fact that the constituent crystallites have a size of ~20 nm.

3.5. Photoluminescence (PL). In Figure 6(a) excitation spectrum of representative $Gd_2Ti_2O_7$:10 at.% Eu^{3+} sample with

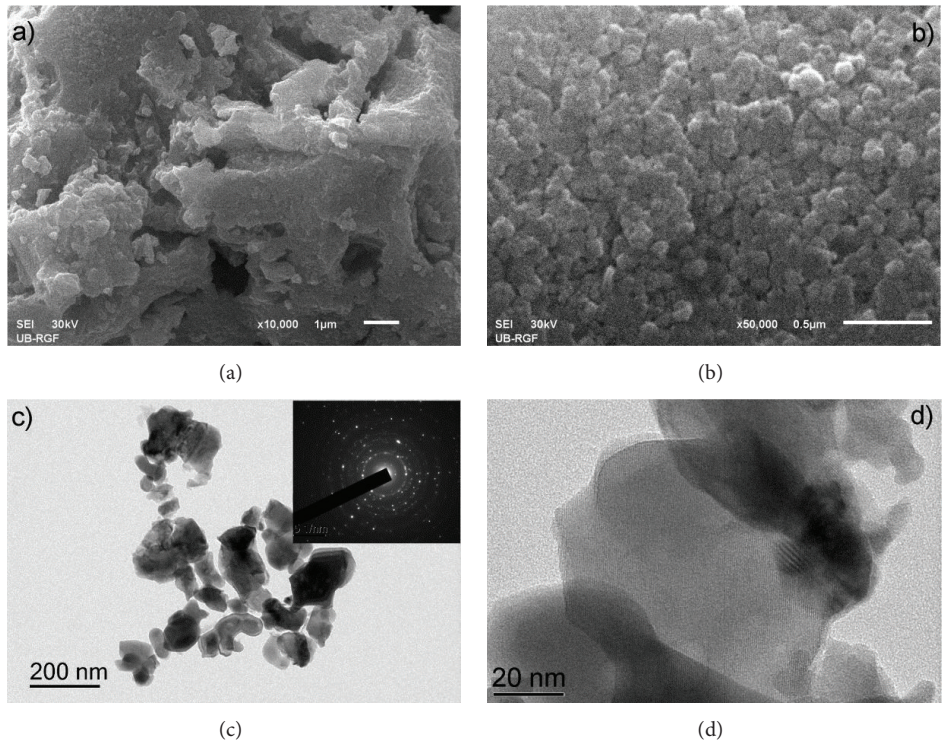

Figure 5: SEM image of 3 at.% Eu^{3+}-doped $Gd_2Ti_2O_7$ nanopowder under (a) low (×10000) and (b) high magnification (×50000). The bright-field TEM images show that (c) most particles have irregular particles size and shape and that (d) nanoparticles are organized in agglomerates, some of which formed the bigger crystals. The SAED diffraction pattern of $Gd_2Ti_2O_7$ presented as an inset in Figure 5(c) shows good crystallinity of the material.

Table 2: Selected structural parameters obtained from XRD measurements.

$Gd_2Ti_2O_7$	a (Å)	Crystallite size (nm)	Microstrain (%)	Rwp (%)	Rp (%)	GOF
0.5 at.% Eu^{3+}	10.1624(4)	17.9(3)	0.23(10)	3.02	2.42	1.0467
1 at.% Eu^{3+}	10.1692(6)	23.8(3)	0.04(8)	3.56	2.75	1.4959
3 at.% Eu^{3+}	10.1714(6)	26.4(3)	0.07(6)	3.76	2.89	1.5241
5 at.% Eu^{3+}	10.1722(4)	25.0(3)	0.12(8)	2.69	2.14	1.1209
7 at.% Eu^{3+}	10.1724(5)	24.7(2)	0.07(6)	2.79	2.21	1.1396
10 at.% Eu^{3+}	10.1731(6)	21.6(4)	0.05(10)	2.86	2.26	1.1435

marked transitions, measured in the spectral region between 325 and 560 nm at room temperature, is presented. Photoluminescence emission spectra of samples with different Eu^{3+} concentration are presented in Figure 6(b). Emission intensity as a function of Eu^{3+} ions concentration (see inset in Figure 6(b)) shows that emission increases with Eu^{3+} doping and that $Gd_2Ti_2O_7$ host can accept Eu^{3+} ions in concentrations up to 10 at.% without concentration quenching. Figures 6(c)-6(d) show more clearly emission spectra of $Gd_2Ti_2O_7$:10 at.% Eu^{3+} and 15 at.% Eu^{3+} samples recorded at room temperature. Excitation into the $^5L_6$ level (λ_{ex} = 393 nm) produces distinct luminescence bands in the visible spectral region. Both spectra show five characteristic bands placed around 579 nm, 589 nm, 612 nm, 652 nm, and 712 nm associated with $^5D_0 \rightarrow {}^7F_J$ ($J = 0, 1, 2, 3, 4$) spin forbidden *f-f* transitions, respectively. However, in the 10 at.% Eu^{3+} spectrum the most intense sharp orange-reddish line placed around 589 nm (magnetic-dipole $^5D_0 \rightarrow {}^7F_1$ transition) is followed by quite broad red emission placed around 612 nm (electric-dipole $^5D_0 \rightarrow {}^7F_2$ transition). On the other hand, in the 15 at.% Eu^{3+} sample spectrum this ratio is inverted. It is generally acknowledged that when a rare-earth ion is situated in a centrosymmetric site then, according to the Laporte rule, only magnetic-dipole transitions are possible. According to Tanner [29] when Eu^{3+} ion is placed in crystallographic site of D_{3d} point symmetry (with a strict center of symmetry) only doublet corresponding to $^5D_0 \rightarrow {}^7F_1$ transition should be visible. Therefore, presence of dominant sharp orange-reddish $^5D_0 \rightarrow {}^7F_1$ doublet in 10 at.% sample suggests a crystalline environment of Eu^{3+} ions and their incorporation into nanoparticles. On the other hand, observation of broad forbidden $^5D_0 \rightarrow {}^7F_J$ ($J = 0, 2, 3, 4$) electric-dipole transitions could be related to the distorted sites near nanoparticle's surface or other defects. Observed most intense $^5D_0 \rightarrow {}^7F_2$ transition in 15 at.% sample clearly indicates presence of additional defects in the structure. Even though XRD

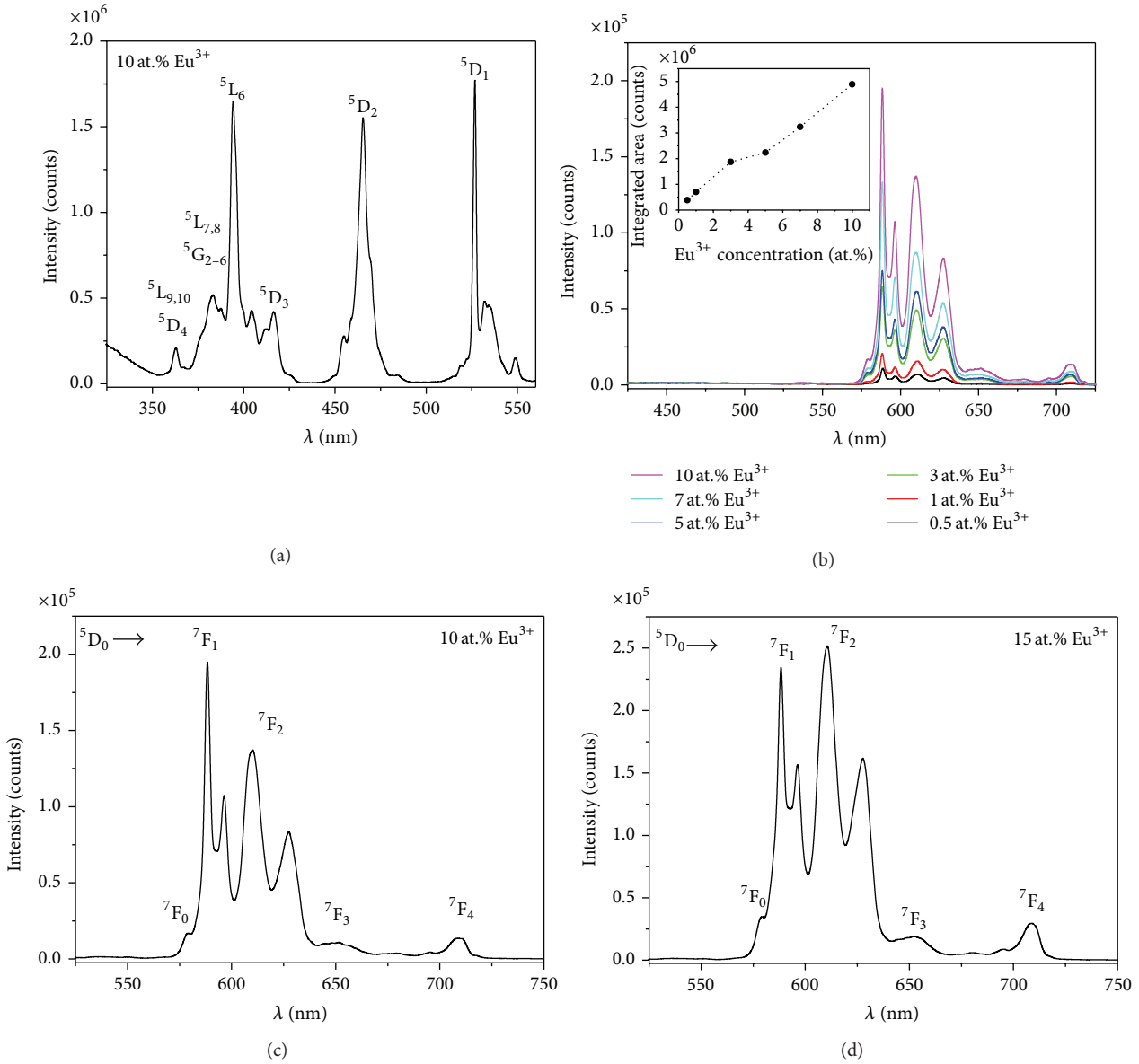

FIGURE 6: (a) Excitation spectrum (λ_{em} = 589 nm) of representative $Gd_2Ti_2O_7$:10 at.% Eu^{3+} sample with marked transitions recorded at room temperature and (b) emission spectra of $Gd_2Ti_2O_7$:x at.% Eu^{3+} (x = 0.5; 1; 3; 5; 7; 10) samples (λ_{exc} = 393 nm) with dependence of the emission intensity versus Eu^{3+} concentration as inset. All spectra were recorded at room temperature and under the same experimental conditions. Photoluminescent emission spectra recorded in the spectral range 525–725 nm at room temperature of (c) $Gd_2Ti_2O_7$:10 at.% Eu^{3+} and (d) $Gd_2Ti_2O_7$:15 at.% Eu^{3+} sample.

spectra showed hardly noticeable difference, photoluminescence spectroscopy clearly revealed presence of additional impurities. This observation indicates that luminescence spectroscopy is an effective method for investigating the presence of defects and could be used as extremely sensitive structural probe technique.

The emission decay curves of the $^5D_0$ emitting level are obtained under excitation at 393 nm (λ_{em} = 588 nm) (see Figure 7(a)) and indicate a complex luminescence decay process. As can be seen, all curves could be fitted with at least two exponential functions. For this reason we found it more appropriate to calculate an average lifetime using the following equation [30]:

$$\tau_{avg} = \frac{\int_0^\infty tI(t)\,dt}{\int_0^\infty I(t)\,dt}, \quad (1)$$

where $I(t)$ represents the luminescence intensity at time t, corrected for the background, and the integrals are evaluated on the range $0 < t < t_m$, where $t_m \gg \tau_{avg}$.

Figure 7(b) shows how the dopant concentration influences lifetime values. Up to 3 at.% Eu^{3+} values are similar experiencing decrease at higher concentrations. Generally, these lifetime values are almost two times shorter than our previous results on the same material obtained by mixed metal-citric acid method [16]. This clearly indicates that sol-gel method produces materials with more defects

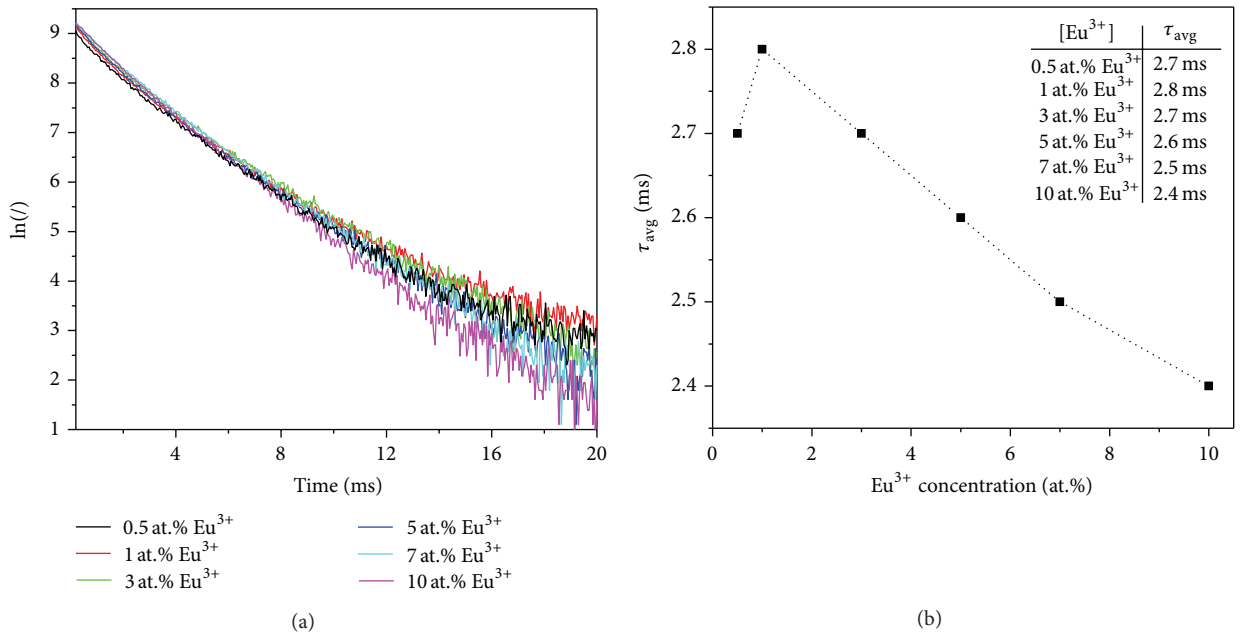

FIGURE 7: (a) Luminescence decay curves of $^5D_0$ level (λ_{em} = 588 nm, λ_{ex} = 393 nm) for $Gd_2Ti_2O_7$:x at.% Eu^{3+} (x = 0.5; 1; 3; 5; 7; 10) samples and (b) change of $^5D_0$ level lifetime with doping concentration.

in the structure and confirms that photoluminescent spectroscopy could be used as a sensitive tool for monitoring structural changes in both steady state and lifetime domains.

4. Conclusion

Eu^{3+}-doped $Gd_2Ti_2O_7$ samples produced via sol-gel synthesis and annealed at 840°C for 4 h were studied in order to observe the dopant's influence on the structural and optical properties. XRD measurements revealed that up to 10 at.% dopant Eu^{3+} ions have been effectively incorporated into the $Gd_2Ti_2O_7$ host lattice while at higher dopant concentrations barely visible traces of impurities are present. Microstructure at a local level revealed that sol-gel synthesis produces particles with well-defined crystallinity and irregular size and shape, organized in agglomerates, some of which formed the big crystals. The dependence of luminescence emission intensity on Eu^{3+} concentration shows that the strongest emission is found for sample containing 10 at.%. On the other hand, with an increase in Eu^{3+} concentration the lifetime of the $^5D_0$ level decreases from ~2.8 ms (for 1 at.% Eu^{3+}) to ~ 2.4 ms (for 10 at.% Eu^{3+}). Correlation between structural and photoluminescent properties reveals that photoluminescent spectroscopy of rare-earths (e.g., Eu^{3+} ions) could be proposed as an effective method for investigating the presence of defects and structural changes in optically active materials.

Conflict of Interests

The authors declare that there is no conflict of interests regarding the publication of this paper.

Acknowledgments

This work is supported by the Ministry of Education, Science and Technological Development of the Republic of Serbia (Grants nos. 172056 and 45020). Authors would like to thank Dr. Phillip S. Ahrenkiel, South Dakota School of Mines & Technology, Rapid City, South Dakota, USA, for transmission electron microscopy images.

References

[1] B. J. Kennedy, B. A. Hunter, and C. J. Howard, "Structural and bonding trends in tin pyrochlore oxides," *Journal of Solid State Chemistry*, vol. 130, no. 1, pp. 58–65, 1997.

[2] H. W. J. Blöte, R. F. Wielinga, and W. J. Huiskamp, "Heat-capacity measurements on rare-earth double oxides $R_2M_2O_7$," *Physica*, vol. 43, no. 4, pp. 549–568, 1969.

[3] S. T. Bramwell, M. N. Field, M. J. Harris, and I. P. Parkin, "Bulk magnetization of the heavy rare earth titanate pyrochlore—a series of model frustrated magnets," *Journal of Physics Condensed Matter*, vol. 12, no. 4, pp. 483–495, 2000.

[4] A. P. Ramirez, "Geometrical frustration," in *Handbook on Magnetic Materials*, K. H. J. Buschow, Ed., vol. 13, p. 423, Elsevier, Amsterdam, The Netherlands, 2001.

[5] C. Heremans, B. J. Wuensch, J. K. Stalick, and E. Prince, "Fast-ion conducting $Y_2(Zr_yTi_{1-y})_2O_7$ pyrochlores: neutron rietveld analysis of disorder induced by Zr substitution," *Journal of Solid State Chemistry*, vol. 117, no. 1, pp. 108–121, 1995.

[6] L. Minervini, R. W. Grimes, K. E. Sickafus, and C. Randall, "Disorder in pyrochlore oxides," *Journal of the American Ceramic Society*, vol. 83, no. 8, pp. 1873–1878, 2000.

[7] C. R. Stanek, L. Minervini, and R. W. Grimes, "Nonstoichiometry in $A_2B_2O_7$ pyrochlores," *Journal of the American Ceramic Society*, vol. 85, no. 11, pp. 2792–2798, 2002.

[8] A. R. Heredia, M. Q. García, J. L. P. Mazariego, and R. Escamilla, "X-ray diffraction and Raman spectroscopy on $Gd_2(Ti_{2-y}Te_y)O_7$ prepared at high pressure and high temperature," *Journal of Alloys and Compounds*, vol. 504, no. 2, pp. 446–451, 2010.

[9] A. F. Fuentes, K. Boulahya, M. MacZka, J. Hanuza, and U. Amador, "Synthesis of disordered pyrochlores, $A_2Ti_2O_7$ (A = Y, Gd and Dy), by mechanical milling of constituent oxides," *Solid State Sciences*, vol. 7, no. 4, pp. 343–353, 2005.

[10] N. P. Raju, M. Dion, M. J. P. Gingras, T. E. Mason, and J. E. Greedan, "Transition to long-range magnetic order in the highly frustrated insulating pyrochlore antiferromagnet $Gd_2Ti_2O_7$," *Physical Review B: Condensed Matter and Materials Physics*, vol. 59, no. 22, pp. 14489–14498, 1999.

[11] K.-M. Lin, C.-C. Lin, C.-Y. Hsiao, and Y.-Y. Li, "Synthesis of $Gd_2Ti_2O_7$:Eu^{3+}, V^{4+} phosphors by sol-gel process and its luminescent properties," *Journal of Luminescence*, vol. 127, no. 2, pp. 561–567, 2007.

[12] L. Lin and B. Yan, "Rare earth titanates ceramics $Na_2La_2Ti_3O_{10}$: Pr^{3+} and $RE_2Ti_2O_7$: Pr^{3+} (R = Gd, Y): sol-gel synthesis, characterization and luminescence," *Journal of Materials Science: Materials in Electronics*, vol. 22, no. 6, pp. 672–678, 2011.

[13] N. Dharuman and L. John Berchmans, "Low temperature synthesis of nano-crystalline gadolinium titanate by molten salt route," *Ceramics International*, vol. 39, no. 8, pp. 8768–8771, 2013.

[14] W. Peng, B. Hu, C. Yan et al., "Hydrothermal synthesis and characterization of pyrochlore titanate $R_2Ti_2O_7$(R=Gd^{3+}, Tb^{3+}, Dy^{3+})," *Chemical Research in Chinese Universities*, vol. 27, no. 2, pp. 161–165, 2011.

[15] W. Zhang, L. Zhang, H. Zhong, L. Lu, X. Yang, and X. Wang, "Synthesis and characterization of ultrafine $Ln_2Ti_2O_7$ (Ln = Sm, Gd, Dy, Er) pyrochlore oxides by stearic acid method," *Materials Characterization*, vol. 61, no. 2, pp. 154–158, 2010.

[16] S. Ćulubrk, Ž. Antić, M. Marinović-Cincović, P. S. Ahrenkiel, and M. D. Dramićanin, "Synthesis and luminescent properties of rare earth (Sm^{3+} and Eu^{3+}) doped $Gd_2Ti_2O_7$ pyrochlore nanopowders," *Optical Materials*, vol. 37, pp. 598–606, 2014.

[17] K. Binnemans and C. Görller-Walrand, "Application of the Eu^{3+} ion for site symmetry determination," *Journal of Rare Earths*, vol. 14, no. 3, pp. 173–180, 1996.

[18] V. Đorđević, Ž. Antić, V. Lojpur, and M. D. Dramićanin, "Europium-doped nanocrystalline Y_2O_3-La_2O_3 solid solutions with bixbyite structure," *Journal of Physics and Chemistry of Solids*, vol. 75, no. 10, pp. 1152–1159, 2014.

[19] M. L. Pang, J. Lin, J. Fu, and Z. Y. Cheng, "Luminescent properties of $Gd_2Ti_2O_7$: Eu^{3+} phosphor films prepared by sol-gel process," *Materials Research Bulletin*, vol. 39, no. 11, pp. 1607–1614, 2004.

[20] K.-M. Lin, C.-C. Lin, and Y.-Y. Li, "Luminescent properties and characterization of $Gd_2O_3Eu^{3+}$@SiO_2 and $Gd_2Ti_2O_7Eu^{3+}$@SiO2 core-shell phosphors prepared by sol-gel process," *Nanotechnology*, vol. 17, no. 6, pp. 1745–1751, 2006.

[21] M. Saif, "Luminescence based on energy transfer in silica doped with lanthanide titania ($Gd_2Ti_2O_7$:Ln^{3+}) [Ln^{3+} = Eu^{3+} or Dy^{3+}]," *Journal of Photochemistry and Photobiology A: Chemistry*, vol. 205, no. 2-3, pp. 145–150, 2009.

[22] Y. Zhang, L. Ding, X. Pang, and W. Zhang, "Influence of annealing temperature on luminescent properties of Eu^{3+}/V^{5+} co-doped nanocrystalline $Gd_2Ti_2O_7$ powders," *Journal of Rare Earths*, vol. 27, no. 6, pp. 900–904, 2009.

[23] Y. Zhang, C. Jia, Z. Su, and W. Zhang, "The enhanced and color-tunable photoluminescence of Eu^{3+}/V^{5+} co-doped $Gd_2Ti_2O_7$ nanocrystals," *Journal of Alloys and Compounds*, vol. 479, no. 1-2, pp. 381–384, 2009.

[24] G. Dagan and M. Tomkiewicz, "Titanium dioxide aerogels for photocatalytic decontamination of aquatic environments," *The Journal of Physical Chemistry*, vol. 97, no. 49, pp. 12651–12655, 1993.

[25] M. Marinović-Cincović, B. Janković, B. Milićević, Ž. Antić, R. K. Whiffen, and M. D. Dramićanin, "The comparative kinetic analysis of the non-isothermal crystallization process of Eu^{3+} doped Zn_2SiO_4 powders prepared via polymer induced sol-gel method," *Powder Technology*, vol. 249, pp. 497–512, 2013.

[26] G. Socrates, *Infrared and Raman Characteristics Group Frequences Tables and Charts*, John Wiley & Sons, West Sussex, UK, 3rd edition, 2001.

[27] M. A. Subramanian, G. Aravamudan, and G. V. Subba Rao, "Oxide pyrochlores—a review," *Progress in Solid State Chemistry*, vol. 15, no. 2, pp. 55–143, 1983.

[28] H. Okamoto, "O-Ti (Oxygen-Titanium)," *Journal of Phase Equilibria and Diffusion*, vol. 32, no. 5, pp. 473–474, 2011.

[29] P. A. Tanner, "Some misconceptions concerning the electronic spectra of tri-positive europium and cerium," *Chemical Society Reviews*, vol. 42, no. 12, pp. 5090–5101, 2013.

[30] E. Nakazawa, "Fundamentals of luminescence," in *Phosphor Handbook*, S. Shionoya and W. M. Yen, Eds., pp. 11–141, CRC Press, New York, NY, USA, 1999.